



# Semileptonic decays $B_c$ meson to S-wave charmonia and $X(3872)$ within the covariant light-front approach

Zhi-Jie Sun<sup>1</sup>, Si-Yang Wang<sup>2</sup>, Zhi-Qing Zhang<sup>1,a</sup>, You-Ya Yang<sup>1</sup>, Zi-Yu Zhang<sup>1</sup>

<sup>1</sup> Institute of Theoretical Physics, School of Sciences, Henan University of Technology, Zhengzhou 450052, Henan, China

<sup>2</sup> Institute of Particle Physics and Key Laboratory of Quark and Lepton Physics (MOE), Central China Normal University, Wuhan 430079, Hubei, China

Received: 7 August 2023 / Accepted: 12 September 2023 / Published online: 20 October 2023  
© The Author(s) 2023

**Abstract** In this work, we investigate the semileptonic decays of  $B_c$  meson to  $\eta_c(1S, 2S, 3S)$ ,  $\psi(1S, 2S, 3S)$  and  $X(3872)$  within the framework of covariant light-front quark model (CLFQM). We combine the helicity amplitudes via the corresponding form factors to obtain the branching ratios of the semileptonic decays  $B_c \rightarrow \eta_c(1S, 2S, 3S)\ell\nu_\ell$ ,  $B_c \rightarrow \psi(1S, 2S, 3S)\ell\nu_\ell$  and  $B_c \rightarrow X(3872)\ell\nu_\ell$ , with  $\ell = e, \mu, \tau$ . In view of the  $R_{J/\psi}$  anomaly released by the LHCb collaboration, it is necessary to systematically calculate the ratios  $R_X$  with  $X = \psi(1S, 2S, 3S)$ ,  $\eta_c(1S, 2S, 3S)$ ,  $X(3872)$ , which are helpful for checking the lepton flavor universality (LFU). We also take into account another two physical observables, the longitudinal polarization fraction  $f_L$  and the forward–backward asymmetry  $A_{FB}$ , which can provide new clues for understanding the  $R_{J/\psi}$  anomaly. Such theoretical predictions are necessary and interesting, and can be tested in future LHCb experiments.

## 1 Introduction

In this paper we investigate the exclusive semileptonic decay of  $B_c$  mesons to  $\eta_c(1S, 2S, 3S)$ ,  $\psi(1S, 2S, 3S)$  and  $X(3872)$  using the covariant light-front quark model (CLFQM). The traditional light-front quark model (LFQM) initially proposed by Terentev and Berestetsky [1–4] is based on the light-front formalism of Hamiltonian dynamics [5], and later developed and applied to determine the transition form factors, decay constants and distribution amplitudes [6–8]. Unfortunately, the Lorentz covariance of the matrix element is lost and the zero-mode contributions cannot be handled in the traditional LFQM. To compensate for these deficiencies, Jaus put forward the CLFQM [9], where the spurious contri-

butions that are dependent on the orientation of the light-front can be eliminated by the inclusion of the zero-mode contributions. This model has been successfully used to investigate the nonleptonic and semileptonic decays of  $B_{(c)}$  mesons [10–14].

The semileptonic decays of  $B_c$  meson to charmonium states plays an important role in testing the Standard Model (SM) and searching for new physics (NP). For example, the testing of lepton flavor universality (LFU) and determination of the Cabibbo–Kobayashi–Maskawa (CKM) matrix element  $V_{cb}$  are investigated both experimentally and theoretically. In 2017, the ratio of the semileptonic branching fractions  $R_{J/\psi}|_{\text{exp}}$  was measured by the Large Hadron Collider beauty (LHCb) collaboration [15],

$$R_{J/\psi}|_{\text{exp}} = \frac{\mathcal{B}r(B_c^+ \rightarrow J/\psi \tau^+ \nu_\tau)}{\mathcal{B}r(B_c^+ \rightarrow J/\psi \mu^+ \nu_\mu)} = 0.71 \pm 0.17 \pm 0.18, \quad (1)$$

which lies within  $2\sigma$  above the range of existing SM predictions [16, 17]. This was considered one of the most fascinating puzzles in flavor physics in recent years. In order to provide a generalized and complementary check, it is useful to measure the values of  $R_{\psi(2S, 3S)}$  and  $R_{\eta_c(1S, 2S, 3S)}$ . At present, there also exist results of these ratios predicted by other approaches. Furthermore, two other physical measurements are also sensitive to NP, namely the longitudinal polarization fraction  $f_L$  and the forward–backward asymmetry  $A_{FB}$ . These observations can be represented by the helicity amplitudes, which are combined via the corresponding form factors.

Many different theoretical methods have been devoted to studying the semileptonic decays of  $B_c$  meson to charmonium states, such as the nonrelativistic QCD (NRQCD) [18, 19], the Bethe–Salpeter (BS) method [20, 21], the relativistic quark model (RQM) [22–24], the light-cone QCD

<sup>a</sup> e-mail: zhangzhiqing@haut.edu.cn (corresponding author)

sum rules [25, 26], the relativistic constituent quark model (RCQM) [27, 28], the non-relativistic quark model (NRQM) [29], the QCD potential model(QCDPM) [30], the Isgur–Scora–Grinstein–Wise (ISGW2) quark model [31], the perturbative QCD (PQCD) approach [32–34], the covariant confined quark model (CCQM) [35], the QCD sum rules (QCDSR) [36], the covariant quark model (CQM) [37] and the relativistic independent quark (RIQ) model [38].

The remainder of this paper is organized as follows. In Sect. 2, the formalism of the CLFQM and the helicity amplitudes combined via form factors are presented. Numerical results for the branching ratios, longitudinal polarization fractions  $f_L$  and forward–backward asymmetries  $A_{FB}$  for these semileptonic  $B_c$  decays are listed in Sect. 3. Detailed comparisons with other theoretical values and relevant discussions are also included. The summary is presented in Sect. 4. Some specific rules when performing the  $p^-$  integration and analytical expressions of the  $B_c \rightarrow \eta_c(1S, 2S, 3S), \psi(1S, 2S, 3S), X(3872)$  transition form factors are collected in Appendix A and B, respectively.

## 2 Formalism

### 2.1 Covariant light-front quark model

In the covariant light-front quark model, we will employ the light-front decomposition of the momentum  $p = (p^-, p^+, p_\perp)$  with  $p^\pm = p^0 \pm p_z, p^2 = p^+ p^- - p_\perp^2$ . The Feynman diagrams for  $B_c$  meson decay and transition amplitudes are shown in Fig. 1. The incoming (outgoing) meson has mass  $M'(M'')$  with momentum  $P' = p'_1 + p_2(P'' = p'_1 + p_2)$ , where  $p'_1$  and  $p_2$  are the momenta of the quark and anti-quark inside the incoming (outgoing) meson with the mass  $m'_1$  and  $m_2$ , respectively. Here we use the same notations as those in Refs. [9, 13], and  $M'$  refers to  $m_{B_c}$  for  $B_c$  meson decays. These momenta can be expressed in terms of the internal variables  $(x_i, p'_\perp)$  as

$$p_{1,2}^+ = x_{1,2} P'^+, \quad p'_{1,2\perp} = x_{1,2} P'_\perp \pm p'_\perp, \tag{2}$$

where  $x_1 + x_2 = 1$ . Using these internal variables, we can define some quantities for the incoming meson which will be used in the following calculations:

$$\begin{aligned} M_0'^2 &= (e'_1 + e_2)^2 = \frac{p_\perp'^2 + m_1'^2}{x_1} + \frac{p_\perp^2 + m_2^2}{x_2}, \\ \tilde{M}'_0 &= \sqrt{M_0'^2 - (m'_1 - m_2)^2}, \\ e_i^{(\prime)} &= \sqrt{m_i^{(\prime)2} + p_\perp'^2 + p_z'^2}, \quad p'_z = \frac{x_2 M'_0}{2} - \frac{m_2^2 + p_\perp'^2}{2x_2 M'_0}, \end{aligned} \tag{3}$$

where  $M'_0$  is the kinetic invariant mass of the incoming meson and can be expressed as the energies of the quark and the anti-quark  $e_i^{(\prime)}$ . It is similar to the case of the outgoing meson. To calculate the amplitudes for the transition form factors, we need the Feynman rules for the meson-quark-antiquark vertices ( $i\Gamma'_M(M = \eta_c, \psi, X)$ ), which can be found in Ref. [39]. Here,  $X(3872)$  is considered as a  $1^{++}$  charmonium state in our calculations and replaced with  $X$  in some places for simplicity.

### 2.2 Helicity amplitudes and observables

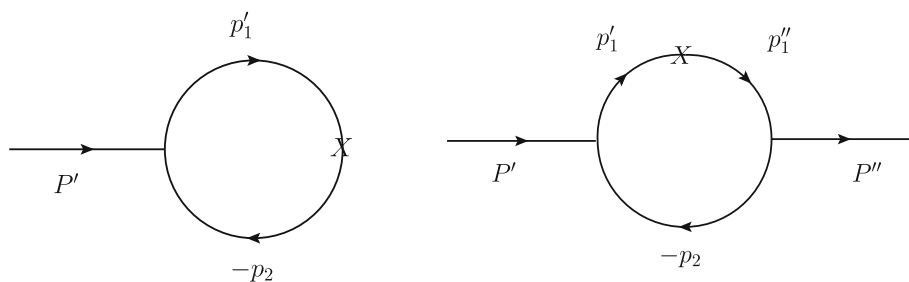
Since the form factors involving the fitted parameters for the  $B_c \rightarrow \eta_c(1S, 2S, 3S), B_c \rightarrow \psi(1S, 2S, 3S)$  and  $B_c \rightarrow X(3872)$  transitions were investigated in our recent work [10], it is convenient to obtain the differential decay widths of these semileptonic decays of  $B_c$  meson by the combination of the helicity amplitudes via form factors, which are listed as follows:

$$\begin{aligned} \frac{d\Gamma(B_c \rightarrow \eta_c \ell \nu_\ell)}{dq^2} &= \left( \frac{q^2 - m_\ell^2}{q^2} \right)^2 \\ &\times \frac{\sqrt{\lambda(m_{B_c}^2, m_{\eta_c}^2, q^2)} G_F^2 |V_{cb}|^2}{384 m_{B_c}^3 \pi^3} \times \frac{1}{q^2} \\ &\times \left\{ (m_\ell^2 + 2q^2) \lambda(m_{B_c}^2, m_{\eta_c}^2, q^2) F_1^2(q^2) + 3m_\ell^2 (m_{B_c}^2 - m_{\eta_c}^2)^2 F_0^2(q^2) \right\}, \end{aligned} \tag{4}$$

$$\begin{aligned} \frac{d\Gamma_L(B_c \rightarrow \psi \ell \nu_\ell)}{dq^2} &= \left( \frac{q^2 - m_\ell^2}{q^2} \right)^2 \\ &\times \frac{\sqrt{\lambda(m_{B_c}^2, m_\psi^2, q^2)} G_F^2 |V_{cb}|^2}{384 m_{B_c}^3 \pi^3} \\ &\times \frac{1}{q^2} \left\{ 3m_\ell^2 \lambda(m_{B_c}^2, m_\psi^2, q^2) A_0^2(q^2) + (m_\ell^2 + 2q^2) \right. \\ &\times \left. \left[ \frac{1}{2m_\psi} \left[ (m_{B_c}^2 - m_\psi^2 - q^2)(m_{B_c} + m_\psi) A_1(q^2) - \frac{\lambda(m_{B_c}^2, m_\psi^2, q^2)}{m_{B_c} + m_\psi} A_2(q^2) \right]^2 \right] \right\}, \end{aligned} \tag{5}$$

$$\begin{aligned} \frac{d\Gamma_\pm(B_c \rightarrow \psi \ell \nu_\ell)}{dq^2} &= \left( \frac{q^2 - m_\ell^2}{q^2} \right)^2 \\ &\times \frac{\sqrt{\lambda(m_{B_c}^2, m_\psi^2, q^2)} G_F^2 |V_{cb}|^2}{384 m_{B_c}^3 \pi^3} \end{aligned}$$

**Fig. 1** Feynman diagrams for  $B_c$  decay (left) and transition (right) amplitudes, where  $P^{(\prime\prime)}$  is the incoming (outgoing) meson momentum,  $p_1^{(\prime\prime)}$  is the quark momentum and  $p_2$  is the anti-quark momentum. The X in the diagrams denotes the vector or axial-vector transition vertex



$$\times \left\{ (m_\ell^2 + 2q^2)\lambda(m_{B_c}^2, m_\psi^2, q^2) \left| \frac{V(q^2)}{m_{B_c} + m_\psi} \mp \frac{(m_{B_c} + m_\psi)A_1(q^2)}{\sqrt{\lambda(m_{B_c}^2, m_\psi^2, q^2)}} \right|^2 \right\}, \tag{6}$$

$$\frac{d\Gamma_L(B_c \rightarrow X\ell\nu_\ell)}{dq^2} = \left( \frac{q^2 - m_\ell^2}{q^2} \right)^2 \times \frac{\sqrt{\lambda(m_{B_c}^2, m_X^2, q^2)}G_F^2|V_{cb}|^2}{384m_{B_c}^3\pi^3} \times \frac{1}{q^2} \left\{ 3m_\ell^2\lambda(m_{B_c}^2, m_X^2, q^2)V_0^2(q^2) + (m_\ell^2 + 2q^2) \times \left[ \frac{1}{2m_X} \left[ (m_{B_c}^2 - m_X^2 - q^2)(m_{B_c} - m_X)V_1(q^2) - \frac{\lambda(m_{B_c}^2, m_X^2, q^2)}{m_{B_c} - m_X}V_2(q^2) \right]^2 \right] \right\}, \tag{7}$$

$$\frac{d\Gamma_\pm(B_c \rightarrow X\ell\nu_\ell)}{dq^2} = \left( \frac{q^2 - m_\ell^2}{q^2} \right)^2 \times \frac{\sqrt{\lambda(m_{B_c}^2, m_X^2, q^2)}G_F^2|V_{cb}|^2}{384m_{B_c}^3\pi^3} \times \left\{ (m_\ell^2 + 2q^2)\lambda(m_{B_c}^2, m_X^2, q^2) \left| \frac{A(q^2)}{m_{B_c} - m_X} \mp \frac{(m_{B_c} - m_X)V_1(q^2)}{\sqrt{\lambda(m_{B_c}^2, m_X^2, q^2)}} \right|^2 \right\}, \tag{8}$$

where  $\lambda(q^2) = \lambda(m_{B_c}^2, m_{\eta_c(\psi, X)}^2, q^2) = (m_{B_c}^2 + m_{\eta_c(\psi, X)}^2 - q^2)^2 - 4m_{B_c}^2 m_{\eta_c(\psi, X)}^2$ , and  $m_\ell$  is the mass of the lepton  $\ell$  with  $\ell = e, \mu, \tau$ .<sup>1</sup> Although the electron and muon are very light compared with the charm quark, we do not ignore their masses in our calculations. The combined transverse and total

differential decay widths are defined as

$$\frac{d\Gamma_T}{dq^2} = \frac{d\Gamma_+}{dq^2} + \frac{d\Gamma_-}{dq^2}, \quad \frac{d\Gamma}{dq^2} = \frac{d\Gamma_L}{dq^2} + \frac{d\Gamma_T}{dq^2}. \tag{9}$$

For  $\psi(1S, 2S, 3S)$  and  $X(3872)$ , it is meaningful to define the polarization fraction due to the existence of different polarizations

$$f_L = \frac{\Gamma_L}{\Gamma_L + \Gamma_+ + \Gamma_-}. \tag{10}$$

As to the forward-backward asymmetry, the analytical expression is defined as [40]

$$A_{FB} = \frac{\int_0^1 \frac{d\Gamma}{d\cos\theta} d\cos\theta - \int_{-1}^0 \frac{d\Gamma}{d\cos\theta} d\cos\theta}{\int_{-1}^1 \frac{d\Gamma}{d\cos\theta} d\cos\theta} = \frac{\int b_\theta(q^2) dq^2}{\Gamma_{B_c}}, \tag{11}$$

where  $\theta$  is the angle between the 3-momenta of the lepton  $\ell$  and the initial  $B_c$  meson in the  $\ell\nu$  rest frame. The function  $b_\theta(q^2)$  represents the angular coefficient and can be written as [40]

$$b_\theta^{(\eta_c)}(q^2) = \frac{G_F^2|V_{cb}|^2}{128\pi^3 m_{B_c}^3} q^2 \sqrt{\lambda(q^2)} \left( 1 - \frac{m_\ell^2}{q^2} \right)^2 \frac{m_\ell^2}{q^2} (H_{V,0}^s H_{V,t}^s), \tag{12}$$

$$b_\theta^{(\psi, X)}(q^2) = \frac{G_F^2|V_{cb}|^2}{128\pi^3 m_{B_c}^3} q^2 \sqrt{\lambda(q^2)} \left( 1 - \frac{m_\ell^2}{q^2} \right)^2 \times \left[ \frac{1}{2} (H_{V,+}^2 - H_{V,-}^2) + \frac{m_\ell^2}{q^2} (H_{V,0} H_{V,t}) \right], \tag{13}$$

where the helicity amplitudes

$$H_{V,0}^s(q^2) = \sqrt{\frac{\lambda(q^2)}{q^2}} F_1(q^2), \tag{14}$$

$$H_{V,t}^s(q^2) = \frac{m_{B_c}^2 - m_{\eta_c}^2}{\sqrt{q^2}} F_0(q^2),$$

for the  $B_c$  to  $\eta_c(1S, 2S, 3S)$  transitions, the helicity amplitudes

$$H_{V,\pm}(q^2) = (m_{B_c} + m_\psi) A_1(q^2) \mp \frac{\sqrt{\lambda(q^2)}}{m_{B_c} + m_\psi} V(q^2),$$

<sup>1</sup> From now on, we use  $\ell$  to represent  $e, \mu, \tau$  and use  $\ell'$  to represent  $e, \mu$  for simplicity.

**Table 1** The values of the input parameters

Mass (GeV)	$m_b = 4.8$ $m_{J/\psi} = 3.0969$ $m_{\eta_c} = 2.9839$	$m_c = 1.4$ $m_{\psi(2S)} = 3.6861$ $m_{\eta_c(2S)} = 3.6375$	$m_e = 0.000511$ $m_{\psi(3S)} = 4.039$ $m_{\eta_c(3S)} = 3.940$	$m_\mu = 0.106$ $M_{B_c} = 6.27447$ $m_{X(3872)} = 3.87165$	$m_\tau = 1.78$
CKM	$V_{cb} = (40.8 \pm 1.4) \times 10^{-3}$	Lifetime	$\tau_{B_c} = (0.510 \pm 0.009) \times 10^{-12}$ s		

$$\begin{aligned}
 H_{V,0}(q^2) &= \frac{m_{B_c} + m_\psi}{2m_\psi\sqrt{q^2}} \left[ - (m_{B_c}^2 - m_\psi^2 - q^2) A_1(q^2) \right. \\
 &\quad \left. + \frac{\lambda(q^2) A_2(q^2)}{(m_{B_c} + m_\psi)^2} \right], \\
 H_{V,i}(q^2) &= -\sqrt{\frac{\lambda(q^2)}{q^2}} A_0(q^2), \tag{15}
 \end{aligned}$$

for the  $B_c$  to  $\psi(1S, 2S, 3S)$  transitions, and the helicity amplitudes

$$\begin{aligned}
 H_{V,\pm}(q^2) &= (m_{B_c} - m_X) V_1(q^2) \mp \frac{\sqrt{\lambda(q^2)}}{m_{B_c} - m_X} A(q^2), \\
 H_{V,0}(q^2) &= \frac{m_{B_c} - m_X}{2m_X\sqrt{q^2}} \left[ - (m_{B_c}^2 - m_X^2 - q^2) V_1(q^2) \right. \\
 &\quad \left. + \frac{\lambda(q^2) V_2(q^2)}{(m_{B_c} - m_X)^2} \right], \\
 H_{V,i}(q^2) &= -\sqrt{\frac{\lambda(q^2)}{q^2}} V_0(q^2), \tag{16}
 \end{aligned}$$

for the  $B_c$  to  $X(3872)$  transition. The subscript  $V$  in each helicity amplitude refers to the  $\gamma_\mu(1 - \gamma_5)$  current. The transition form factors are collected in Appendix B.

### 3 Numerical results and discussion

The input parameters adopted in our numerical calculations [41], including the constituent quark masses, the hadron and lepton masses, the  $B_c$  meson lifetime and the CKM matrix element  $V_{cb}$ , are listed in Table 1. In the calculations of the helicity amplitudes, the transition form factors are the most important inputs, and they were calculated in our previous work [10]. Those parameterized form factors are extrapolated from the space-like region to the time-like region using the following expression.

$$F(q^2) = F(0) \exp \left( a \frac{q^2}{m_{B_c}^2} + b \left( \frac{q^2}{m_{B_c}^2} \right)^2 \right), \tag{17}$$

Here,  $F(q^2)$  denotes different form factors. Compared with other parameterization forms, this formula is more accurate, where the parameters  $a, b$  can be well determined with

smaller relative errors. The corresponding results are listed in Table 2.

The branching ratios for these semileptonic  $B_c$  decays to the S-wave ground charmonium states are collected in Table 3. The uncertainties arise from the  $B_c$  meson lifetime and the decay constants of final-state mesons, respectively. Obviously, because the mass of the  $\tau$  lepton is much larger than that of  $e, \mu$  leptons,  $Br(B_c^+ \rightarrow \eta_c(J/\Psi)\ell'^+\nu_{\ell'})$  are about 3 ~ 4 times larger than  $Br(B_c^+ \rightarrow \eta_c(J/\Psi)\tau^+\nu_\tau)$ . For comparison, we also list the results calculated by other approaches. The predictions given by the NRQCD [18, 19] and the PQCD approach [32] are much larger than others, as the former involves the large QCD correction K factor and the next-to-leading-order (NLO) charmonium wave functions, and the latter includes the large weak transition form factors. These differences can be clarified by future LHCb experiments. Certainly, our predictions are consistent with most other theoretical results, such as the BS equation [20], the RQM [22–24], the RCQM [27, 28], the NRQM [29], the QCDDM [30] and the CQM [37].

From Table 3, it can be seen that the value of the ratio  $R_{J/\psi}$

$$R_{J/\psi} = \frac{Br(B_c^+ \rightarrow J/\psi\tau^+\nu_\tau)}{Br(B_c^+ \rightarrow J/\psi\mu^+\nu_\mu)} = 0.25 \pm 0.04, \tag{18}$$

which falls within the range of  $0.24 \leq R_{J/\psi} \leq 0.28$  predicted by most other SM approaches, and is also consistent with the model-independent constraint  $0.20 \leq R_{J/\psi} \leq 0.39$  [16]. Our prediction is smaller than the measured one shown in Eq. (1), but still agrees with it within  $2\sigma$  errors. As a complementary check, we also calculate the value of  $R_{\eta_c}$ ,

$$R_{\eta_c} = \frac{Br(B_c^+ \rightarrow \eta_c\tau^+\nu_\tau)}{Br(B_c^+ \rightarrow \eta_c\mu^+\nu_\mu)} = 0.29 \pm 0.02, \tag{19}$$

which is still consistent with most of the other theoretical results lying in the range of  $0.25 \leq R_{\eta_c} \leq 0.35$  [42, 43], and agrees well with the model-independent prediction  $0.29 \pm 0.05$  [44].

The branching ratios of the semileptonic  $B_c$  decays to the radially excited charmonium states are shown in Table 4, together with the results obtained in other approaches for comparison. The uncertainties are the same as those shown in Table 3. It is observed that the large errors in the  $B_c^+ \rightarrow \eta_c(2S)\ell^+\nu_\ell$  decays are induced by the decay con-

**Table 2**  $B_c \rightarrow \eta_c(1S, 2S, 3S), \psi(1S, 2S, 3S), X(3872)$  form factors in the CLFQM. The uncertainties are from the decay constants of  $B_c$  and the final-state mesons

$B_c \rightarrow \eta_c$		$B_c \rightarrow J/\psi$				
	$F_1$	$F_0$	$V$	$A_0$	$A_1$	$A_2$
$F(0)$	$0.60^{+0.00+0.01}_{-0.00-0.01}$	$0.60^{+0.00+0.01}_{-0.01-0.00}$	$0.76^{+0.00+0.04}_{-0.00-0.04}$	$0.55^{+0.00+0.03}_{-0.00-0.04}$	$0.53^{+0.00+0.02}_{-0.03-0.00}$	$0.49^{+0.00+0.00}_{-0.00-0.01}$
$F(q_{max}^2)$	$1.06^{+0.00+0.03}_{-0.00-0.03}$	$0.85^{+0.00+0.02}_{-0.01-0.02}$	$1.37^{+0.00+0.11}_{-0.00-0.10}$	$0.76^{+0.00+0.06}_{-0.00-0.07}$	$0.78^{+0.01+0.02}_{-0.01-0.05}$	$0.84^{+0.00+0.03}_{-0.00-0.00}$
$a$	$1.95^{+0.01+0.03}_{-0.01-0.03}$	$1.44^{+0.00+0.03}_{-0.00-0.03}$	$2.16^{+0.01+0.09}_{-0.01-0.08}$	$1.22^{+0.02+0.07}_{-0.02-0.07}$	$1.45^{+0.03+0.09}_{-0.01-0.09}$	$1.97^{+0.01+0.11}_{-0.01-0.11}$
$b$	$0.48^{+0.00+0.01}_{-0.00-0.01}$	$-0.62^{+0.02+0.02}_{-0.02-0.03}$	$0.53^{+0.00+0.01}_{-0.00-0.01}$	$0.16^{+0.00+0.00}_{-0.00-0.00}$	$0.29^{+0.00+0.02}_{-0.00-0.00}$	$0.43^{+0.00+0.03}_{-0.00-0.03}$
$B_c \rightarrow \eta_c(2S)$		$B_c \rightarrow \psi(2S)$				
	$F_1$	$F_0$	$V$	$A_0$	$A_1$	$A_2$
$F(0)$	$0.37^{+0.00+0.12}_{-0.00-0.18}$	$0.37^{+0.00+0.12}_{-0.00-0.18}$	$0.57^{+0.00+0.01}_{-0.00-0.00}$	$0.41^{+0.00+0.00}_{-0.00-0.00}$	$0.35^{+0.00+0.00}_{-0.00-0.00}$	$0.17^{+0.00+0.00}_{-0.00-0.00}$
$F(q_{max}^2)$	$0.48^{+0.00+0.28}_{-0.00-0.31}$	$0.41^{+0.00+0.28}_{-0.01-0.28}$	$0.67^{+0.00+0.02}_{-0.00-0.00}$	$0.44^{+0.00+0.00}_{-0.00-0.00}$	$0.35^{+0.00+0.00}_{-0.00-0.00}$	$0.12^{+0.00+0.00}_{-0.00-0.00}$
$a$	$1.44^{+0.00+0.92}_{-0.00-0.66}$	$0.73^{+0.01+0.99}_{-0.01-0.95}$	$1.01^{+0.01+0.01}_{-0.01-0.02}$	$0.39^{+0.01+0.01}_{-0.01-0.01}$	$0.08^{+0.01+0.02}_{-0.02-0.03}$	$-1.53^{+0.07+0.09}_{-0.09-0.13}$
$b$	$0.15^{+0.02+0.50}_{-0.02-0.34}$	$-0.81^{+0.02+0.34}_{-0.02-0.28}$	$-0.16^{+0.03+0.01}_{-0.03-0.02}$	$-0.15^{+0.02+0.01}_{-0.02-0.01}$	$-0.69^{+0.03+0.01}_{-0.04-0.02}$	$-3.67^{+0.14+0.13}_{-0.19-0.21}$
$B_c \rightarrow \eta_c(3S)$		$B_c \rightarrow \psi(3S)$				
	$F_1$	$F_0$	$V$	$A_0$	$A_1$	$A_2$
$F(0)$	$0.29^{+0.00+0.04}_{-0.00-0.05}$	$0.29^{+0.00+0.04}_{-0.00-0.05}$	$0.46^{+0.00+0.02}_{-0.00-0.02}$	$0.31^{+0.00+0.01}_{-0.00-0.01}$	$0.27^{+0.00+0.01}_{-0.00-0.01}$	$0.14^{+0.00+0.01}_{-0.00-0.01}$
$F(q_{max}^2)$	$0.36^{+0.00+0.07}_{-0.00-0.08}$	$0.32^{+0.00+0.07}_{-0.00-0.08}$	$0.53^{+0.00+0.03}_{-0.00-0.03}$	$0.33^{+0.00+0.01}_{-0.00-0.01}$	$0.28^{+0.00+0.02}_{-0.00-0.01}$	$0.12^{+0.00+0.02}_{-0.00-0.02}$
$a$	$1.53^{+0.00+0.29}_{-0.00-0.23}$	$0.85^{+0.01+0.44}_{-0.01-0.31}$	$1.14^{+0.03+0.04}_{-0.03-0.03}$	$0.49^{+0.03+0.03}_{-0.02-0.03}$	$0.25^{+0.02+0.04}_{-0.02-0.03}$	$-1.01^{+0.02+0.04}_{-0.02-0.04}$
$b$	$0.23^{+0.01+0.13}_{-0.01-0.13}$	$-0.74^{+0.01+0.05}_{-0.00-0.24}$	$-0.01^{+0.01+0.01}_{-0.01-0.01}$	$-0.04^{+0.01+0.01}_{-0.01-0.01}$	$-0.45^{+0.01+0.00}_{-0.01-0.00}$	$-2.73^{+0.01+0.00}_{-0.01-0.00}$
$B_c \rightarrow X(3872)$		$A$	$V_0$	$V_1$	$V_2$	
$F(0)$		$0.28^{+0.00+0.02}_{-0.00-0.03}$	$0.21^{+0.00+0.01}_{-0.00-0.01}$	$1.13^{+0.00+0.01}_{-0.00-0.03}$	$0.11^{+0.00+0.01}_{-0.01-0.01}$	
$F(q_{max}^2)$		$0.37^{+0.00+0.03}_{-0.00-0.04}$	$0.19^{+0.00+0.02}_{-0.00-0.02}$	$1.10^{+0.00+0.05}_{-0.00-0.06}$	$0.12^{+0.00+0.01}_{-0.01-0.01}$	
$a$		$1.85^{+0.02+0.09}_{-0.02-0.08}$	$-0.52^{+0.01+0.38}_{-0.01-0.32}$	$-0.05^{+0.01+0.24}_{-0.01-0.20}$	$0.77^{+0.03+0.04}_{-0.03-0.04}$	
$b$		$0.38^{+0.01+0.01}_{-0.01-0.03}$	$-1.45^{+0.02+0.36}_{-0.03-0.32}$	$-1.03^{+0.00+0.15}_{-0.00-0.12}$	$-0.61^{+0.02+0.08}_{-0.02-0.12}$	

stant  $f_{\eta_c(2S)} = (243^{+79}_{-111})$  MeV [10]. For the  $B_c^+ \rightarrow \eta_c(2S)\ell^+\nu_\ell, \psi(2S)\ell^+\nu_\ell$  decays, their branching ratios are much smaller than the PQCD calculations [32]. Our predictions are consistent with the results given by the BS equation [20], the light-cone QCD sum rules [25] and the ISGW2 quark model [31]. Although the results for the semileptonic  $B_c$  decays to the ground-state charmonia given by the relativistic quark model [22,23] are appropriate, those for the semileptonic  $B_c$  decays to the radially excited charmonium states given by such approach seem to be too small. The branching ratios of these semileptonic decays show a clear hierarchical relationship,

$$Br(B_c \rightarrow \eta_c(3S)\ell\nu_\ell) < Br(B_c \rightarrow \eta_c(2S)\ell\nu_\ell) < Br(B_c \rightarrow \eta_c(1S)\ell\nu_\ell), \tag{20}$$

$$Br(B_c \rightarrow \psi(3S)\ell\nu_\ell) < Br(B_c \rightarrow \psi(2S)\ell\nu_\ell) < Br(B_c \rightarrow \psi(1S)\ell\nu_\ell). \tag{21}$$

This is mainly because the relationships  $m_{\eta_c(1S)} < m_{\eta_c(2S)} < m_{\eta_c(3S)}$  and  $m_{\psi(1S)} < m_{\psi(2S)} < m_{\psi(3S)}$  lead to a decrease

in the phase spaces of the final states with the increase in the radial quantum number  $n$ .

Similar to  $R_{J/\psi}$ , it is useful to define the ratios of the branching ratios for the  $B_c$  decays to the radially excited charmonia, where the uncertainties induced by the model calculations and the CKM matrix elements can be canceled

$$R_{\psi(nS)} = \frac{Br(B_c^+ \rightarrow \psi(nS)\tau^+\nu_\tau)}{Br(B_c^+ \rightarrow \psi(nS)\mu^+\nu_\mu)},$$

$$R_{\eta_c(nS)} = \frac{Br(B_c^+ \rightarrow \eta_c(nS)\tau^+\nu_\tau)}{Br(B_c^+ \rightarrow \eta_c(nS)\mu^+\nu_\mu)}, \tag{22}$$

where  $n = 2, 3$ . Our predictions  $R_X$  with  $X = \eta_c(1S, 2S, 3S), \psi(1S, 2S, 3S)$  are collected in Table 5, together with the results obtained in other approaches for comparison. Obviously, it shows a clear hierarchical relationship,

$$R_{\psi(3S)} < R_{\psi(2S)} < R_{J/\psi}, \quad R_{\eta_c(3S)} < R_{\eta_c(2S)} < R_{\eta_c(1S)}. \tag{23}$$

**Table 3** Branching ratios (in%) of the semileptonic  $B_c$  decays to  $\eta_c$  and  $J/\Psi$

	$Br(B_c^+ \rightarrow \eta_c e^+ \nu_e)$	$Br(B_c^+ \rightarrow \eta_c \mu^+ \nu_\mu)$	$Br(B_c^+ \rightarrow \eta_c \tau^+ \nu_\tau)$	$Br(B_c^+ \rightarrow J/\psi e^+ \nu_e)$	$Br(B_c^+ \rightarrow J/\psi \mu^+ \nu_\mu)$	$Br(B_c^+ \rightarrow J/\psi \tau^+ \nu_\tau)$
This work	$0.71^{+0.01+0.03}_{-0.01-0.03}$	$0.69^{+0.01+0.03}_{-0.01-0.03}$	$0.20^{+0.00+0.01}_{-0.00-0.01}$	$1.60^{+0.03+0.19}_{-0.03-0.04}$	$1.59^{+0.03+0.19}_{-0.03-0.04}$	$0.40^{+0.01+0.05}_{-0.01-0.02}$
[18, 19]	2.1	2.1	0.64	6.7	6.7	0.52
[20]	0.55	–	–	1.73	–	–
[22, 23]	0.42	–	–	1.23	–	–
[24]	0.81	–	0.22	2.07	–	0.49
[26]	1.64	–	0.49	2.37	–	0.65
[11]	0.67	0.67	0.19	1.49	1.49	0.37
[29]	0.48	0.48	0.17	1.54	1.54	0.41
[30]	0.15	–	–	1.5	–	–
[37]	0.95	0.95	0.24	1.67	1.67	0.40
[32]	4.5	4.5	2.8	5.7	5.7	1.7
[35]	0.98	–	0.27	2.30	–	0.59
[36, 52]	0.75	0.75	0.23	1.9	1.9	0.48
[53]	0.97	–	–	2.35	–	–
[27, 28]	0.59	0.59	0.20	1.20	1.20	0.34
[33]	0.44	0.44	0.14	1.01	1.01	0.29
[54]	0.42	0.42	0.16	1.31	1.30	0.37

**Table 4** Branching ratios of the semileptonic  $B_c$  decays to the radially excited charmonium states

References	This work	[20]	[22, 23]	[25]	[30]	[31]	[32]
$10^{-3} \times Br(B_c^+ \rightarrow \eta_c(2S)e^+ \nu_e)$	$0.91^{+0.02+0.87}_{-0.02-0.69}$	0.7	0.32	1.1	0.2	0.46	7.7
$10^{-3} \times Br(B_c^+ \rightarrow \eta_c(2S)\mu^+ \nu_\mu)$	$0.91^{+0.02+0.87}_{-0.02-0.69}$	–	–	–	–	–	–
$10^{-5} \times Br(B_c^+ \rightarrow \eta_c(2S)\tau^+ \nu_\tau)$	$8.22^{+0.14+7.37}_{-0.14-6.52}$	–	–	8.1	–	1.3	53
$10^{-3} \times Br(B_c^+ \rightarrow \eta_c(3S)e^+ \nu_e)$	$0.33^{+0.01+0.11}_{-0.01-0.11}$	–	0.0055	0.19	–	–	1.4
$10^{-3} \times Br(B_c^+ \rightarrow \eta_c(3S)\mu^+ \nu_\mu)$	$0.33^{+0.01+0.11}_{-0.01-0.11}$	–	–	–	–	–	–
$10^{-5} \times Br(B_c^+ \rightarrow \eta_c(3S)\tau^+ \nu_\tau)$	$0.39^{+0.01+0.13}_{-0.01-0.12}$	–	0.0005	0.57	–	–	0.19
$10^{-3} \times Br(B_c^+ \rightarrow \psi(2S)e^+ \nu_e)$	$2.34^{+0.04+0.09}_{-0.04-0.02}$	1	0.31	–	1.2	2.1	12
$10^{-3} \times Br(B_c^+ \rightarrow \psi(2S)\mu^+ \nu_\mu)$	$2.32^{+0.04+0.09}_{-0.04-0.02}$	–	–	–	–	–	–
$10^{-5} \times Br(B_c^+ \rightarrow \psi(2S)\tau^+ \nu_\tau)$	$15.89^{+0.28+0.09}_{-0.28-0.20}$	–	–	–	–	15	84
$10^{-3} \times Br(B_c^+ \rightarrow \psi(3S)e^+ \nu_e)$	$0.73^{+0.01+0.05}_{-0.01-0.05}$	–	0.0057	–	–	–	0.36
$10^{-3} \times Br(B_c^+ \rightarrow \psi(3S)\mu^+ \nu_\mu)$	$0.72^{+0.01+0.05}_{-0.01-0.05}$	–	–	–	–	–	–
$10^{-5} \times Br(B_c^+ \rightarrow \psi(3S)\tau^+ \nu_\tau)$	$0.58^{+0.01+0.03}_{-0.01-0.02}$	–	0.0036	–	–	–	0.038

It can be seen from Table 5 that our predictions for these  $R$  values are comparable to other SM calculations. If a departure of the SM predictions for  $R_{\psi(2S,3S)}$  and  $R_{\eta_c(1S,2S,3S)}$  from the experimental data can be detected, it will further highlight the puzzle in flavor physics and the failure of lepton flavor universality suggested in the  $R_{J/\psi}$  measurement [15]. Our predictions for the branching ratios of these semileptonic  $B_c$  decays to the radially excited charmonia are larger than  $10^{-6}$ , which can be measured in future high-luminosity LHC (HL-LHC) and high-energy LHC (HE-LHC) experiments [45]. Then, the semileptonic  $B_c$  decays to the ground and excited charmonia will provide a more complete research area.

In order to investigate the impact of the lepton masses and provide a more detailed physical picture for the semileptonic  $B_c$  decays beyond the branching ratio, we also define another two physical observations that can be measured by experiments: the longitudinal polarization fraction  $f_L$  and the forward–backward asymmetry  $A_{FB}$ . These two physical quantities are sensitive to some new physics [46–50], so their values are helpful for testing the SM and different NP scenarios. Meanwhile, the calculations of these two quantities may provide new clues to understanding the puzzle of the  $R_{J/\psi}$  ratio. We expect that these physical observables can be measured by future LHCb experiments, and will be helpful



**Table 5** The values of ratios  $R_X$  with  $X = \eta_c(1S, 2S, 3S), \psi(1S, 2S, 3S)$

Ratio	This work	[38]	[24]	[21]	[33]	[22,23]	[34]	[37]	[25]	[31]
$R_{\eta_c}$	$0.29 \pm 0.02$	–	0.27	–	0.31	–	–	0.25	–	–
$R_{\eta_c(2S)}$	$0.09 \pm 0.12$	0.14	–	0.054	–	–	0.069	–	0.74	0.028
$R_{\eta_c(3S)}$	$0.012 \pm 0.006$	0.021	–	0.010	–	0.0010	0.0014	–	0.03	–
$R_{J/\psi}$	$0.25 \pm 0.04$	–	0.24	–	0.29	–	–	0.24	–	–
$R_{\psi(2S)}$	$0.068 \pm 0.003$	0.085	–	0.51	–	–	0.070	–	–	0.071
$R_{\psi(3S)}$	$0.0081 \pm 0.0007$	0.078	–	0.0092	–	0.0063	0.0011	–	–	–

**Table 6** The longitudinal polarization fractions  $f_L$  (in%) for the decays  $B_c^+ \rightarrow \eta_c(1S, 2S, 3S)\ell^+ \nu_\ell, B_c^+ \rightarrow \psi(1S, 2S, 3S)\ell^+ \nu_\ell$ . The uncertainties are the same as those given in Table 3

Decay modes	$B_c^+ \rightarrow J/\psi e^+ \nu_e$	$B_c^+ \rightarrow J/\psi \mu^+ \nu_\mu$	$B_c^+ \rightarrow J/\psi \tau^+ \nu_\tau$
This work	$50.9^{+0.9+5.5}_{-0.9-5.1}$	$50.9^{+0.9+5.7}_{-0.9-5.2}$	$43.8^{+0.8+5.6}_{-0.8-5.1}$
[32]	33	33	39
[54]	44	44	40
[11]	51	51	45
Decay modes	$B_c^+ \rightarrow \psi(2S) e^+ \nu_e$	$B_c^+ \rightarrow \psi(2S) \mu^+ \nu_\mu$	$B_c^+ \rightarrow \psi(2S) \tau^+ \nu_\tau$
This work	$59.2^{+1.0+0.1}_{-1.0-0.2}$	$59.2^{+1.0+0.1}_{-1.0-0.2}$	$44.6^{+0.8+0.2}_{-0.8-0.3}$
[32]	46	46	41
Decay modes	$B_c^+ \rightarrow \psi(3S) e^+ \nu_e$	$B_c^+ \rightarrow \psi(3S) \mu^+ \nu_\mu$	$B_c^+ \rightarrow \psi(3S) \tau^+ \nu_\tau$
This work	$57.9^{+1.0+4.0}_{-1.0-4.1}$	$57.9^{+1.0+4.0}_{-1.0-4.1}$	$40.5^{+0.7+3.2}_{-0.7-3.1}$
[32]	54	54	31

for clarifying the discrepancies among different theoretical approaches. From the numerical results listed in Tables 6 and 8, the following points can be found:

(1) From Eqs. (7)–(10), we find that the longitudinal polarization fractions  $f_L$  of the decays  $B_c^+ \rightarrow J/\psi \ell^+ \nu_\ell$  decrease with the increase in  $m_\ell$ , although this trend is mild, that is,

$$f_L(B_c^+ \rightarrow J/\psi e^+ \nu_e) \approx f_L(B_c^+ \rightarrow J/\psi \mu^+ \nu_\mu) > f_L(B_c^+ \rightarrow J/\psi \tau^+ \nu_\tau), \tag{24}$$

which is supported by our predictions shown in Table 6. Certainly, this rule can also be applied to the decays  $B_c^+ \rightarrow \psi(2S, 3S)\ell^+ \nu_\ell$ .

In order to investigate the dependence of the polarization on the different  $q^2$ , we calculate the longitudinal polarization fractions by dividing the full energy region into two regions for each decay, which are listed in Table 7 together with the partial branching ratios, where Region 1 is defined as  $m_\ell^2 < q^2 < \frac{(m_{B_c} - m_{\psi(nS)})^2 + m_\ell^2}{2}$  and Region 2 is  $\frac{(m_{B_c} - m_{\psi(nS)})^2 + m_\ell^2}{2} < q^2 < (m_{B_c} - m_{\psi(nS)})^2$ , with  $n = 1, 2, 3$ . From Table 7 we can see that in Region 1, the longitudinal polarizations dominate the branching ratios for the decays with  $e$  and  $\mu$  involved, while the longitudinal and

transverse polarizations for the decay channels involving  $\tau$  are comparable in Region 1. It is interesting that for all the considered decays, the transverse polarizations dominate in Region 2. These results can be tested by future LHCb experiments.

(2) From Table 8, we find that the ratios of the forward–backward asymmetries  $A_{FB}$  between the different semileptonic decays associated with the  $B_c \rightarrow \eta_c(nS)$  transitions have the following rules:  $A_{FB}^\mu/A_{FB}^e = (3 \sim 4) \times 10^4$  and  $A_{FB}^\tau/A_{FB}^e > 1 \times 10^5$ . This is because  $A_{FB}$  for  $B_c \rightarrow \eta_c(nS)$  transitions is proportional to the square of the lepton mass shown in Eqs. (11)–(12). Undoubtedly, the effect of lepton mass can be confirmed in such decay modes with the pseudoscalar mesons involved in the final states. For the  $B_c \rightarrow \psi(nS)$  transitions, the values of the forward–backward asymmetries  $A_{FB}^\mu$  are almost equal to  $A_{FB}^e$ , while the values of  $A_{FB}^\tau$  are smaller than those of  $A_{FB}^{e(\mu)}$ . The dominant contribution to the  $A_{FB}$  for the  $B_c \rightarrow \psi(nS)$  transitions arises from the term proportional to  $(H_{V,+}^2 - H_{V,-}^2)$  in Eq. (13).

In Figs. 2 and 3, we display the  $q^2$  dependence of the differential decay rates  $d\Gamma_{(L)}/dq^2$  and the forward–backward asymmetries  $A_{FB}$ , respectively. It can be observed that the values of  $d\Gamma_{(L)}/dq^2$  and  $A_{FB}$  coincide with 0 at the zero

**Table 7** The partial branching ratios and longitudinal polarization fraction  $f_L(\text{in}\%)$  for the decays  $B_c^+ \rightarrow \eta_c(1S, 2S, 3S)\ell^+\nu_\ell$ ,  $B_c^+ \rightarrow \psi(1S, 2S, 3S)\ell^+\nu_\ell$  in Region 1 and Region 2

Observables	Region 1	Region 2	Observables	Region 1	Region 2	Observables	Region 1	Region 2
$\mathcal{B}r(B_c^+ \rightarrow J/\psi e^+\nu_e)$	$0.71 \times 10^{-2}$	$0.89 \times 10^{-2}$	$\mathcal{B}r(B_c^+ \rightarrow J/\psi \mu^+\nu_\mu)$	$0.71 \times 10^{-2}$	$0.88 \times 10^{-2}$	$\mathcal{B}r(B_c^+ \rightarrow J/\psi \tau^+\nu_\tau)$	$0.13 \times 10^{-2}$	$0.27 \times 10^{-2}$
$f_L(B_c^+ \rightarrow J/\psi e^+\nu_e)$	64.5	40.1	$f_L(B_c^+ \rightarrow J/\psi \mu^+\nu_\mu)$	64.5	40.1	$f_L(B_c^+ \rightarrow J/\psi \tau^+\nu_\tau)$	53.9	40.1
$\mathcal{B}r(B_c^+ \rightarrow \psi(2S)e^+\nu_e)$	$1.33 \times 10^{-3}$	$1.01 \times 10^{-3}$	$\mathcal{B}r(B_c^+ \rightarrow \psi(2S)\mu^+\nu_\mu)$	$1.31 \times 10^{-3}$	$1.01 \times 10^{-3}$	$\mathcal{B}r(B_c^+ \rightarrow \psi(2S)\tau^+\nu_\tau)$	$5.33 \times 10^{-5}$	$10.55 \times 10^{-5}$
$f_L(B_c^+ \rightarrow \psi(2S)e^+\nu_e)$	71.2	43.4	$f_L(B_c^+ \rightarrow \psi(2S)\mu^+\nu_\mu)$	71.2	43.5	$f_L(B_c^+ \rightarrow \psi(2S)\tau^+\nu_\tau)$	52.4	40.7
$\mathcal{B}r(B_c^+ \rightarrow \psi(3S)e^+\nu_e)$	$0.40 \times 10^{-3}$	$0.33 \times 10^{-3}$	$\mathcal{B}r(B_c^+ \rightarrow \psi(3S)\mu^+\nu_\mu)$	$0.40 \times 10^{-3}$	$0.33 \times 10^{-3}$	$\mathcal{B}r(B_c^+ \rightarrow \psi(3S)\tau^+\nu_\tau)$	$0.16 \times 10^{-5}$	$0.42 \times 10^{-5}$
$f_L(B_c^+ \rightarrow \psi(3S)e^+\nu_e)$	70.2	42.8	$f_L(B_c^+ \rightarrow \psi(3S)\mu^+\nu_\mu)$	70.2	42.9	$f_L(B_c^+ \rightarrow \psi(3S)\tau^+\nu_\tau)$	45.7	38.1

**Table 8** The forward–backward asymmetries  $A_{FB}$  for the decays  $B_c^+ \rightarrow \eta_c(1S, 2S, 3S)\ell^+\nu_\ell$  and  $B_c^+ \rightarrow \psi(1S, 2S, 3S)\ell^+\nu_\ell$

Decay modes	$B_c^+ \rightarrow \eta_c e^+\nu_e$	$B_c^+ \rightarrow \eta_c \mu^+\nu_\mu$	$B_c^+ \rightarrow \eta_c \tau^+\nu_\tau$
This work	$(3.93^{+0.07+0.14}_{-0.07-0.01}) \times 10^{-7}$	$0.015^{+0.000+0.001}_{-0.000-0.000}$	$0.36^{+0.01+0.02}_{-0.01-0.01}$
[54]	$-8.6 \times 10^{-7}$	-0.012	-0.35
[55]	$-2.049 \times 10^{-7}$	-	0.357
[56]	-	-	0.364
Decay modes	$B_c^+ \rightarrow \eta_c(2S)e^+\nu_e$	$B_c^+ \rightarrow \eta_c(2S)\mu^+\nu_\mu$	$B_c^+ \rightarrow \eta_c(2S)\tau^+\nu_\tau$
This work	$(6.96^{+0.12+5.69}_{-0.12-5.17}) \times 10^{-7}$	$0.023^{+0.000+0.019}_{-0.000-0.017}$	$0.30^{+0.01+0.28}_{-0.01-0.24}$
[38]	$5.75 \times 10^{-7}$	-	0.384
Decay modes	$B_c^+ \rightarrow \eta_c(3S)e^+\nu_e$	$B_c^+ \rightarrow \eta_c(3S)\mu^+\nu_\mu$	$B_c^+ \rightarrow \eta_c(3S)\tau^+\nu_\tau$
This work	$(9.00^{+0.16+2.77}_{-0.16-2.88}) \times 10^{-7}$	$0.028^{+0.000+0.009}_{-0.000-0.009}$	$0.33^{+0.01+0.14}_{-0.01-0.12}$
[38]	$10.5 \times 10^{-7}$	-	0.367
Decay modes	$B_c^+ \rightarrow J/\psi e^+\nu_e$	$B_c^+ \rightarrow J/\psi \mu^+\nu_\mu$	$B_c^+ \rightarrow J/\psi \tau^+\nu_\tau$
This work	$-0.21^{+0.00+0.02}_{-0.00-0.02}$	$-0.21^{+0.00+0.02}_{-0.00-0.02}$	$-0.14^{+0.00+0.02}_{-0.00-0.02}$
[54]	-0.19	-0.19	-0.23
[55]	0.18	-	-0.255
[56]	-	-	-0.042
Decay modes	$B_c^+ \rightarrow \psi(2S)e^+\nu_e$	$B_c^+ \rightarrow \psi(2S)\mu^+\nu_\mu$	$B_c^+ \rightarrow \psi(2S)\tau^+\nu_\tau$
This work	$-0.16^{+0.00+0.00}_{-0.00-0.01}$	$-0.16^{+0.00+0.00}_{-0.00-0.01}$	$-0.093^{+0.002+0.014}_{-0.002-0.003}$
[38]	-0.246	-	-0.214
Decay modes	$B_c^+ \rightarrow \psi(3S)e^+\nu_e$	$B_c^+ \rightarrow \psi(3S)\mu^+\nu_\mu$	$B_c^+ \rightarrow \psi(3S)\tau^+\nu_\tau$
This work	$-0.14^{+0.00+0.01}_{-0.00-0.01}$	$-0.14^{+0.00+0.01}_{-0.00-0.01}$	$-0.048^{+0.001+0.014}_{-0.001-0.003}$
[38]	-0.155	-	-0.144

recoil point ( $q^2 = q_{max}^2$ ), since the coefficient  $\lambda(q^2) = \lambda(m_{B_c}^2, m_{\eta_c/\psi}^2, q^2)$  shown in Eqs. (4)–(13) at the same zero recoil point being equal to 0. Furthermore, it is very different for the  $q^2$  dependence of the differential decay rates from the longitudinal polarization  $d\Gamma_L/dq^2$  between the decays  $B_c^+ \rightarrow J/\psi \ell^+\nu_{\ell'}$  and  $B_c^+ \rightarrow \psi(2S, 3S)\ell^+\nu_{\ell'}$ .

We similarly analyze the semileptonic  $B_c^+ \rightarrow X(3872)\ell^+\nu_\ell$  decay by assuming that  $X(3872)$  is a regular  $c\bar{c}$  charmonium state. The branching ratios, longitudinal polariza-

tion fractions  $f_L$  and forward–backward asymmetries  $A_{FB}$  are listed in Table 9. One can observe that  $\mathcal{B}r(B_c^+ \rightarrow X(3872)\tau^+\nu_\tau)$  is only about 1/25th of  $\mathcal{B}r(B_c^+ \rightarrow X(3872)\ell^+\nu_{\ell'})$  due to the narrower phase space of the final states with the  $\tau$  lepton involved. Obviously, our predictions are consistent with those given in the generalized factorization approach (GFA) [51], while they are about 7 ~ 9 times smaller than those in the QCDSR approach [25]. The ratio



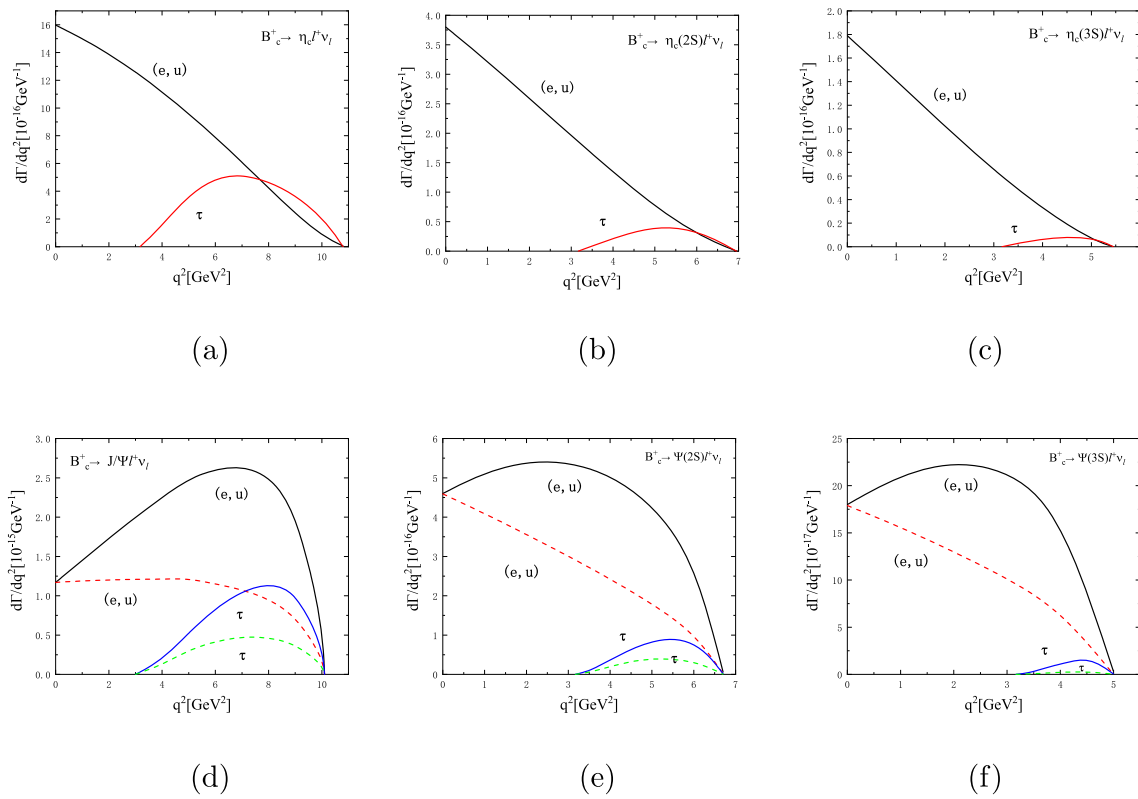


**Fig. 2** The  $q^2$  dependence of the differential decay rates  $d\Gamma/dq^2$  (solid lines) and  $d\Gamma_L/dq^2$  (dashed lines), with  $L$  representing the contribution from the longitudinal polarization

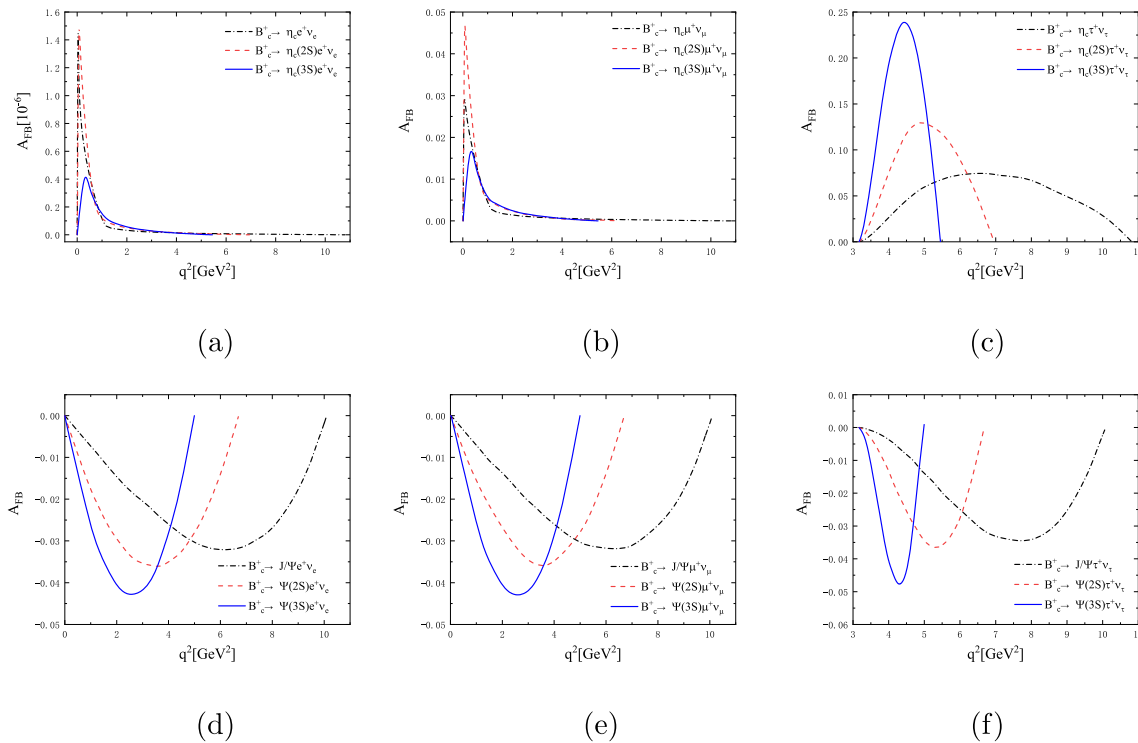


**Fig. 3** The  $q^2$  dependence of the forward–backward asymmetries  $A_{FB}$  for the decays  $B_c \rightarrow \eta_c(1S, 2S, 3S)\ell^+\nu_\ell$  and  $B_c \rightarrow \psi(1S, 2S, 3S)\ell^+\nu_\ell$

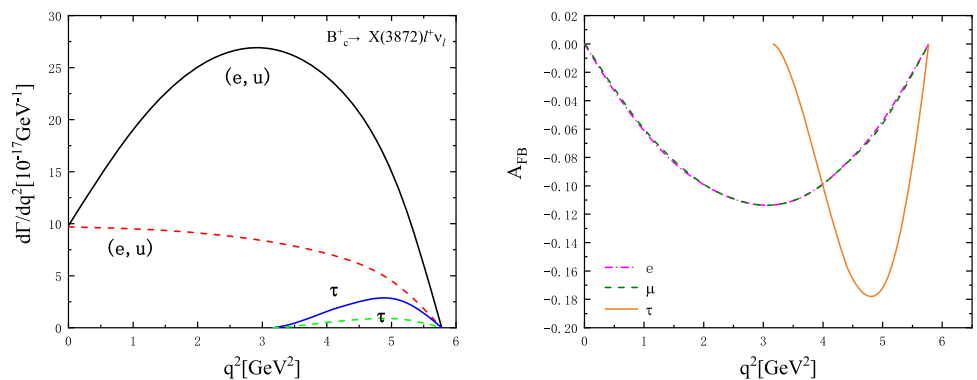
**Table 9** The branching ratios, the longitudinal polarization fractions  $f_L$  and the forward–backward asymmetries  $A_{FB}$  for the semileptonic decays  $B_c^+ \rightarrow X(3872)\ell^+\nu_\ell$

Decay Modes	$Br(10^{-4})$			$f_L(\%)$	$A_{FB}$
	This work	[51]	[25]		
$B_c^+ \rightarrow X(3872)e^+\nu_e$	$9.27^{+0.16+0.01+0.58}_{-0.16-0.22-0.89}$	13.5	67	$36.7^{+0.6+0.0+2.5}_{-0.6-0.1-1.3}$	$-0.45^{+0.01+0.00+0.07}_{-0.01-0.00-0.05}$
$B_c^+ \rightarrow X(3872)\mu^+\nu_\mu$	$9.20^{+0.16+0.01+0.57}_{-0.16-0.21-0.89}$	13.5	–	$36.7^{+0.6+0.0+2.5}_{-0.6-0.0-1.3}$	$-0.44^{+0.01+0.00+0.07}_{-0.01-0.00-0.05}$
$B_c^+ \rightarrow X(3872)\tau^+\nu_\tau$	$0.37^{+0.01+0.00+0.04}_{-0.01-0.00-0.04}$	0.65	3.2	$31.9^{+0.6+0.1+2.6}_{-0.6-0.5-3.1}$	$-0.28^{+0.01+0.00+0.05}_{-0.01-0.00-0.04}$

**Table 10** The partial branching ratios and the longitudinal polarization fraction  $f_L$  (in%) for the decays  $B_c^+ \rightarrow X(3872)\ell^+\nu_\ell$

Observables	Region 1	Region 2	Observables	Region 1	Region 2	Observables	Region 1	Region 2
$Br(B_c^+ \rightarrow X(3872)e^+\nu_e)$	$0.47 \times 10^{-3}$	$0.46 \times 10^{-3}$	$Br(B_c^+ \rightarrow X(3872)\mu^+\nu_\mu)$	$0.46 \times 10^{-3}$	$0.46 \times 10^{-3}$	$Br(B_c^+ \rightarrow X(3872)\tau^+\nu_\tau)$	$1.15 \times 10^{-5}$	$2.58 \times 10^{-5}$
$f_L(B_c^+ \rightarrow X(3872)e^+\nu_e)$	43.4	29.9	$f_L(B_c^+ \rightarrow X(3872)\mu^+\nu_\mu)$	43.4	29.9	$f_L(B_c^+ \rightarrow X(3872)\tau^+\nu_\tau)$	32.3	31.7

**Fig. 4** The  $q^2$  dependence of the differential decay rates  $d\Gamma/dq^2$  (solid lines) and  $d\Gamma_L/dq^2$  (dashed lines) are shown on the left panel and the  $q^2$  dependence of the forward–backward asymmetries  $A_{FB}$  for the decays  $B_c^+ \rightarrow X(3872)\ell^+\nu_\ell$  are shown on the right pannel



$R_X$  is

$$R_X = \frac{Br(B_c^+ \rightarrow X(3872)\tau^+\nu_\tau)}{Br(B_c^+ \rightarrow X(3872)\mu^+\nu_\mu)} = 0.040 \pm 0.006, \quad (25)$$

which is consistent with the value  $R_X = 0.048$  given by the GFA and QCDSR. There is a significant difference in polarization fractions between  $B_c^+ \rightarrow X(3872)\ell^+\nu_\ell$  and  $B_c^+ \rightarrow J/\psi\ell^+\nu_\ell$ : the transverse polarization is dominant in the former, while the longitudinal and transverse polarizations are comparable in the latter. Both the  $B_c^+ \rightarrow X(3872)\tau^+\nu_\tau$  and  $B_c^+ \rightarrow J/\Psi\tau^+\nu_\tau$  decays are dominated by the transverse polarization. The forward–backward asymmetries  $A_{FB}$  of the decays  $B_c^+ \rightarrow X(3872)\ell^+\nu_\ell$  are about twice as large in magnitude as those for the channels  $B_c^+ \rightarrow J/\Psi\ell^+\nu_\ell$ .

The partial branching ratios and longitudinal polarization fractions in Region 1 and Region 2 defined in the previous section are given in Table 10, where the transverse polarizations are dominant in both cases. It is evident that the dominant contributions arise from the transverse polarizations whether in Region 1, Region 2, or the entire physical region. All of these values are meaningful for determining the inner structure of the X(3872) by comparison with future experimental measurements.

In Fig. 4, we plot the  $q^2$  dependence of the differential decay rates  $d\Gamma_{(L)}/dq^2$  with L referring to the longitudinal polarization and the forward–backward asymmetries  $A_{FB}$  for the decays  $B_c^+ \rightarrow X(3872)\ell^+\nu_\ell$ , where it is similar in character to the cases of  $B_c^+ \rightarrow \psi(nS)\ell^+\nu_\ell$ ; that is, the values of  $d\Gamma_{(L)}/dq^2$  and  $A_{FB}$  are coincident with 0 at the zero recoil point ( $q^2 = q_{max}^2$ ). Furthermore, the differential decay rate from the transverse polarization  $d\Gamma_T/dq^2(B_c^+ \rightarrow X(3872)\ell^+\nu_\ell)$  is much more sensitive to the change in  $q^2$  compared with that from the longitudinal polarization  $d\Gamma_L/dq^2(B_c^+ \rightarrow X(3872)\ell^+\nu_\ell)$ .

### 4 Summary

In this work, we investigated the exclusive semileptonic  $B_c$  decays to  $\eta_c(1S, 2S, 3S)$ ,  $\psi(1S, 2S, 3S)$  and X(3872) in the CLFQM. Using the helicity amplitudes combined via the form factors, we calculated the branching ratios, the longitudinal polarization fractions  $f_L$  and the forward–backward asymmetries  $A_{FB}$  for these semileptonic  $B_c$  decays. From the numerical results, we found the following points:

1. Comparing the branching ratios of these semileptonic decays, it shows a clear hierarchical relationship,

$$\begin{aligned} \mathcal{B}r(B_c \rightarrow \eta_c(3S)\ell\nu_\ell) &< \mathcal{B}r(B_c \rightarrow \eta_c(2S)\ell\nu_\ell) \\ &< \mathcal{B}r(B_c \rightarrow \eta_c\ell\nu_\ell), \end{aligned} \tag{26}$$

$$\begin{aligned} \mathcal{B}r(B_c \rightarrow \psi(3S)\ell\nu_\ell) \\ &< \mathcal{B}r(B_c \rightarrow \psi(2S)\ell\nu_\ell) < \mathcal{B}r(B_c \rightarrow J/\Psi\ell\nu_\ell). \end{aligned} \tag{27}$$

2. The ratios  $R_X = \frac{\mathcal{B}r(B_c^+ \rightarrow X\tau^+\nu_\tau)}{\mathcal{B}r(B_c^+ \rightarrow X\mu^+\nu_\mu)}$  are predicted as

$$\begin{aligned} R_{J/\Psi} &= 0.25 \pm 0.04, R_{\psi(2S)} = 0.068 \pm 0.003, \\ R_{\psi(3S)} &= 0.0081 \pm 0.0007, \end{aligned} \tag{28}$$

$$\begin{aligned} R_{\eta_c} &= 0.29 \pm 0.02, R_{\eta_c(2S)} = 0.09 \pm 0.12, \\ R_{\eta_c(3S)} &= 0.012 \pm 0.006, \end{aligned} \tag{29}$$

$$R_{X(3872)} = 0.040 \pm 0.006. \tag{30}$$

3. The longitudinal polarization fractions  $f_L$  for the decays  $B_c^+ \rightarrow \psi\ell^+\nu_\ell$  have the following rules

$$\begin{aligned} f_L(B_c^+ \rightarrow \psi(nS)e^+\nu_e) &\approx f_L(B_c^+ \rightarrow \psi(nS)\mu^+\nu_\mu) \\ &> f_L(B_c^+ \rightarrow \psi(nS)\tau^+\nu_\tau). \end{aligned} \tag{31}$$

The longitudinal polarization dominates the branching ratios for the decays with  $e$  and  $\mu$  involved, while the transverse polarization is dominant for the decays with  $\tau$  involved. It is different for the decays  $B_c^+ \rightarrow X(3872)\ell^+\nu_\ell$ , where the transverse polarization is dominant in all cases.

4. The ratios of the forward–backward asymmetries  $A_{FB}$  between the different semileptonic decays associated with the  $B_c \rightarrow \eta_c(nS)$  transitions are given as

$$\frac{A_{FB}^\mu}{A_{FB}^e} = (3 \sim 4) \times 10^4, \quad \frac{A_{FB}^\tau}{A_{FB}^e} > 1 \times 10^5. \tag{32}$$

While the forward–backward asymmetries  $A_{FB}$  for the decays  $B_c^+ \rightarrow \psi(nS)\ell^+\nu_\ell$  and  $B_c^+ \rightarrow X(3872)\ell^+\nu_\ell$  become minus in sign, the differences between these values  $A_{FB}^\ell$  are small and less than three times.

5. Our predictions are helpful for testing the standard model and different new physics scenarios. Certainly, the values correlated with the  $X(3872)$  are also meaningful for determining the inner structure of the  $X(3872)$  by comparison with future experimental measurements.

**Acknowledgements** This work is partly supported by the National Natural Science Foundation of China under Grant no. 11347030, the Program of Science and Technology Innovation Talents in Universities of Henan Province 14HASTIT037, as well as the Natural Science Foundation of Henan Province under Grant no. 232300420116.

**Data Availability Statement** This manuscript has no associated data or the data will not be deposited. [Authors’ comment: This work is a theoretical study. No relevant data to deposit.]

**Open Access** This article is licensed under a Creative Commons Attribution 4.0 International License, which permits use, sharing, adaptation, distribution and reproduction in any medium or format, as long as you give appropriate credit to the original author(s) and the source, provide a link to the Creative Commons licence, and indicate if changes were made. The images or other third party material in this article are included in the article’s Creative Commons licence, unless indicated otherwise in a credit line to the material. If material is not included in the article’s Creative Commons licence and your intended use is not permitted by statutory regulation or exceeds the permitted use, you will need to obtain permission directly from the copyright holder. To view a copy of this licence, visit <http://creativecommons.org/licenses/by/4.0/>.

Funded by SCOAP<sup>3</sup>. SCOAP<sup>3</sup> supports the goals of the International Year of Basic Sciences for Sustainable Development.

### Appendix A: Some specific rules under the $p^-$ integration

When performing the integration, we must include the zero-mode contributions, which amounts to performing the integration in a proper way in the CLFQM. Specifically, we use the following rules given in Refs. [9, 13]

$$\hat{p}'_{1\mu} \doteq P_\mu A_1^{(1)} + q_\mu A_2^{(1)}, \tag{A1}$$

$$\begin{aligned} \hat{p}'_{1\mu}\hat{p}'_{1\nu} &\doteq g_{\mu\nu}A_1^{(2)} + P_\mu P_\nu A_2^{(2)} + (P_\mu q_\nu + q_\mu P_\nu) A_3^{(2)} \\ &\quad + q_\mu q_\nu A_4^{(2)}, \end{aligned} \tag{A2}$$

$$\begin{aligned} Z_2 &= \hat{N}'_1 + m_1'^2 - m_2^2 + (1 - 2x_1) M'^2 \\ &\quad + \left(q^2 + q \cdot P\right) \frac{p'_\perp \cdot q_\perp}{q^2}, \end{aligned} \tag{A3}$$

$$\begin{aligned} A_1^{(1)} &= \frac{x_1}{2}, \quad A_2^{(1)} = A_1^{(1)} - \frac{p'_\perp \cdot q_\perp}{q^2}, \\ A_3^{(2)} &= A_1^{(1)} A_2^{(1)}, \end{aligned} \tag{A4}$$

$$\begin{aligned} A_4^{(2)} &= \left(A_2^{(1)}\right)^2 - \frac{1}{q^2} A_1^{(2)}, \quad A_1^{(2)} = -p_\perp'^2 \\ &\quad - \frac{(p'_\perp \cdot q_\perp)^2}{q^2}, \quad A_2^{(2)} = \left(A_1^{(1)}\right)^2. \end{aligned} \tag{A5}$$

### Appendix B: Expressions of $B_c \rightarrow P, V, A$ form factors

The following are the analytical expressions of the  $B_c \rightarrow \eta_c(1S, 2S, 3S), \psi(1S, 2S, 3S), X(3872)$  transition form factors in the covariant light-front quark model

$$\begin{aligned} F_1^{B_c\eta_c}(q^2) &= \frac{N_c}{16\pi^3} \int dx_2 d^2 p'_\perp \frac{h'_{B_c} h''_{\eta_c}}{x_2 \hat{N}'_1 \hat{N}''_1} \\ &\quad \times \left[ x_1 (M_0'^2 + M_0''^2) + x_2 q^2 - x_2 (m'_1 - m''_1)^2 \right. \\ &\quad \left. - x_1 (m'_1 - m_2)^2 - x_1 (m''_1 - m_2)^2 \right] \end{aligned} \tag{B1}$$

$$\begin{aligned}
 F_0^{B_c \eta_c}(q^2) &= F_1^{B_c \eta_c}(q^2) + \frac{q^2}{(q \cdot P)} \frac{N_c}{16\pi^3} \int dx_2 d^2 p'_\perp \\
 &\times \frac{2h'_{B_c} h''_{\eta_c}}{x_2 \hat{N}'_1 \hat{N}''_1} \left\{ -x_1 x_2 M'^2 - p'^2_\perp - m'_1 m_2 \right. \\
 &+ (m''_1 - m_2) (x_2 m'_1 + x_1 m_2) \\
 &+ 2 \frac{q \cdot P}{q^2} \left( p'^2_\perp + 2 \frac{(p'_\perp \cdot q_\perp)^2}{q^2} \right) \\
 &+ 2 \frac{(p'_\perp \cdot q_\perp)^2}{q^2} - \frac{p'_\perp \cdot q_\perp}{q^2} \\
 &\times [M''^2 - x_2 (q^2 + q \cdot P) - (x_2 - x_1) M'^2 \\
 &+ 2x_1 M_0'^2 - 2(m'_1 - m_2)(m'_1 + m''_1)] \left. \right\}, \tag{B2}
 \end{aligned}$$

$$\begin{aligned}
 V^{B_c \psi}(q^2) &= \frac{N_c(M' + M'')}{16\pi^3} \int dx_2 d^2 p'_\perp \frac{2h'_{B_c} h''_\psi}{x_2 \hat{N}'_1 \hat{N}''_1} \\
 &\times \left\{ x_2 m'_1 + x_1 m_2 + (m'_1 - m''_1) \frac{p'_\perp \cdot q_\perp}{q^2} v \right. \\
 &+ \left. \frac{2}{w''_V} \left[ p'^2_\perp + \frac{(p'_\perp \cdot q_\perp)^2}{q^2} \right] \right\}, \tag{B3}
 \end{aligned}$$

$$\begin{aligned}
 A_1^{B_c \psi}(q^2) &= -\frac{1}{M' + M''} \frac{N_c}{16\pi^3} \int dx_2 d^2 p'_\perp \frac{h'_{B_c} h''_\psi}{x_2 \hat{N}'_1 \hat{N}''_1} \\
 &\times \{ 2x_1 (m_2 - m'_1) (M_0'^2 + M_0''^2) - 4x_1 m'_1 M_0'^2 \\
 &+ 2x_2 m'_1 q \cdot P + 2m_2 q^2 - 2x_1 m_2 (M'^2 + M''^2) \\
 &+ 2(m'_1 - m_2)(m'_1 + m''_1)^2 + 8(m'_1 - m_2) \\
 &\times \left[ p'^2_\perp + \frac{(p'_\perp \cdot q_\perp)^2}{q^2} \right] + 2(m'_1 + m''_1) \\
 &\times (q^2 + q \cdot P) \frac{p'_\perp \cdot q_\perp}{q^2} \\
 &- 4 \frac{q^2 p'^2_\perp + (p'_\perp \cdot q_\perp)^2}{q^2 w''_\psi} \\
 &\times [2x_1 (M'^2 + M_0'^2) - q^2 - q \cdot P \\
 &- 2(q^2 + q \cdot P) \frac{p'_\perp \cdot q_\perp}{q^2} \\
 &- 2(m'_1 - m''_1)(m'_1 - m_2)] \left. \right\}, \tag{B4}
 \end{aligned}$$

$$\begin{aligned}
 A_2^{B_c \psi}(q^2) &= \frac{N_c(M' + M'')}{16\pi^3} \int dx_2 d^2 p'_\perp \frac{2h'_{B_c} h''_\psi}{x_2 \hat{N}'_1 \hat{N}''_1} \\
 &\times \{ (x_1 - x_2) (x_2 m'_1 + x_1 m_2) \\
 &- \frac{p'_\perp \cdot q_\perp}{q^2} [2x_1 m_2 + m''_1 \\
 &+ (x_2 - x_1) m'_1] - 2 \frac{x_2 q^2 + p'_\perp \cdot q_\perp}{x_2 q^2 w''_\psi} \\
 &\times [p'_\perp \cdot p''_\perp + (x_1 m_2 + x_2 m'_1) (x_1 m_2 - x_2 m''_1)] \left. \right\}, \tag{B5}
 \end{aligned}$$

$$A_0^{B_c \psi}(q^2) = \frac{M' + M''}{2M''} A_1^{B_c \psi}(q^2) - \frac{M' - M''}{2M''} A_2^{B_c \psi}(q^2)$$

$$\begin{aligned}
 &- \frac{q^2}{2M''} \frac{N_c}{16\pi^3} \int dx_2 d^2 p'_\perp \frac{h'_{B_c} h''_\psi}{x_2 \hat{N}'_1 \hat{N}''_1} \left\{ 2(2x_1 - 3) \right. \\
 &\times (x_2 m'_1 + x_1 m_2) - 8(m'_1 - m_2) \\
 &\times \left[ \frac{p'^2_\perp}{q^2} + 2 \frac{(p'_\perp \cdot q_\perp)^2}{q^4} \right] - \left[ (14 - 12x_1) m'_1 s \right. \\
 &- 2m''_1 - (8 - 12x_1) m_2 \left. \right] \frac{p'_\perp \cdot q_\perp}{q^2} \\
 &+ \frac{4}{w''_\psi} \left( [M'^2 + M''^2 - q^2 + 2(m'_1 - m_2)(m''_1 + m_2)] \right. \\
 &\times (A_3^{(2)} + A_4^{(2)} - A_2^{(1)}) + Z_2 (3A_2^{(1)} - 2A_4^{(2)} - 1) \\
 &+ \left. \frac{1}{2} \left[ x_1 (q^2 + q \cdot P) - 2M'^2 - 2p'_\perp \cdot q_\perp \right. \right. \\
 &- 2m'_1 (m''_1 + m_2) - 2m_2 (m'_1 - m_2) \left. \left. \right] (A_1^{(1)} + A_2^{(1)} - 1) \right. \\
 &\left. \left. \times q \cdot P \left[ \frac{p'^2_\perp}{q^2} + \frac{(p'_\perp \cdot q_\perp)^2}{q^4} \right] \times (4A_2^{(1)} - 3) \right) \right\}, \tag{B6}
 \end{aligned}$$

$$\begin{aligned}
 A^{B_c X}(q^2) &= (M' - M'') \frac{N_c}{16\pi^3} \int dx_2 d^2 p'_\perp \frac{2h'_{B_c} h''_X}{x_2 \hat{N}'_1 \hat{N}''_1} \\
 &\times \left\{ x_2 m'_1 + x_1 m_2 + (m'_1 + m''_1) \frac{p'_\perp \cdot q_\perp}{q^2} \right. \\
 &+ \left. \frac{2}{w''_X} \left[ p'^2_\perp + \frac{(p'_\perp \cdot q_\perp)^2}{q^2} \right] \right\}, \tag{B7}
 \end{aligned}$$

$$\begin{aligned}
 V_1^{B_c X}(q^2) &= -\frac{1}{M' - M''} \frac{N_c}{16\pi^3} \int dx_2 d^2 p'_\perp \frac{h'_{B_c} h''_X}{x_2 \hat{N}'_1 \hat{N}''_1} \\
 &\times \{ 2x_1 (m_2 - m'_1) (M_0'^2 + M_0''^2) + 4x_1 m'_1 M_0'^2 \\
 &+ 2x_2 m'_1 q \cdot P + 2m_2 q^2 - 2x_1 m_2 (M'^2 + M''^2) \\
 &+ 2(m'_1 - m_2)(m'_1 - m''_1)^2 + 8(m'_1 - m_2) \\
 &\times \left[ p'^2_\perp + \frac{(p'_\perp \cdot q_\perp)^2}{q^2} \right] + 2(m'_1 - m''_1) \\
 &\times (q^2 + q \cdot P) \frac{p'_\perp \cdot q_\perp}{q^2} \\
 &- 4 \frac{q^2 p'^2_\perp + (p'_\perp \cdot q_\perp)^2}{q^2 w''_X} \\
 &\times [2x_1 (M'^2 + M_0'^2) - q^2 - q \cdot P - 2 \\
 &\times (q^2 + q \cdot P) \frac{p'_\perp \cdot q_\perp}{q^2} \\
 &- 2(m'_1 + m''_1)(m'_1 - m_2)] \left. \right\}, \tag{B8}
 \end{aligned}$$

$$\begin{aligned}
 V_2^{B_c X}(q^2) &= (M' - M'') \frac{N_c}{16\pi^3} \int dx_2 d^2 p'_\perp \frac{2h'_{B_c} h''_X}{x_2 \hat{N}'_1 \hat{N}''_1} \\
 &\times \left\{ (x_1 - x_2) (x_2 m'_1 + x_1 m_2) - [2x_1 m_2 - m''_1 \right.
 \end{aligned}$$

$$\begin{aligned}
 & + (x_2 - x_1) m'_1] \times \frac{p'_\perp \cdot q_\perp}{q^2} \\
 & - 2 \frac{x_2 q^2 + p'_\perp \cdot q_\perp}{x_2 q^2 w'_X} [p'_\perp \cdot p''_\perp + (x_1 m_2 + x_2 m'_1) \\
 & \times (x_1 m_2 + x_2 m'_1)], \tag{B9} \\
 V_0^{B_c X}(q^2) = & \frac{M' - M''}{2M''} V_1^{B_c X}(q^2) - \frac{M' + M''}{2M''} V_2^{B_c}(q^2) \\
 & - \frac{q^2}{2M''} \frac{N_c}{16\pi^3} \int dx_2 d^2 p'_\perp \frac{h'_{B_c} h''_X}{x_2 \hat{N}'_1 \hat{N}''_1} \\
 & \times [2(2x_1 - 3)(x_2 m'_1 + x_1 m_2) - 8(m'_1 - m_2) \\
 & \times \left[ \frac{p'^2_\perp}{q^2} + 2 \frac{(p'_\perp \cdot q_\perp)^2}{q^4} \right] - [(14 - 12x_1) m'_1 \\
 & + 2m''_1 - (8 - 12x_1) m_2] \frac{p'_\perp \cdot q_\perp}{q^2} \\
 & + \frac{4}{w''_X} \left( \left[ M'^2 + M''^2 - q^2 \right. \right. \\
 & \left. \left. + 2(m'_1 - m_2)(-m''_1 + m_2) \right] \right. \\
 & \times (A_3^{(2)} + A_4^{(2)} - A_2^{(1)}) \\
 & \left. + Z_2(3A_2^{(1)} - 2A_4^{(2)} - 1) \right. \\
 & \left. + \frac{1}{2} \left[ x_1(q^2 + q \cdot P) - 2M'^2 - 2p'_\perp \cdot q_\perp \right. \right. \\
 & \left. \left. - 2m'_1(-m''_1 + m_2) - 2m_2(m'_1 - m_2) \right] \right. \\
 & \left. \times (A_1^{(1)} + A_2^{(1)} - 1) \right. \\
 & \left. \times q \cdot P \left[ \frac{p'^2_\perp}{q^2} + \frac{(p'_\perp \cdot q_\perp)^2}{q^4} \right] (4A_2^{(1)} - 3) \right] \Bigg\}. \tag{B10}
 \end{aligned}$$

**References**

1. M.V. Terentev, Sov. J. Nucl. Phys. **24**, 106 (1976)
2. M.V. Terentev, Yad. Fiz. **24**, 207 (1976)
3. V.B. Berestetsky, M.V. Terentev, Sov. J. Nucl. Phys. **25**, 347 (1977)
4. V.B. Berestetsky, M.V. Terentev, Yad. Fiz. **25**, 653 (1977)
5. P.A. Dirac, Rev. Mod. Phys. **21**, 392 (1949)
6. W. Jaus, Phys. Rev. D **41**, 3394 (1990)
7. W. Jaus, Phys. Rev. D **44**, 2851 (1991)
8. H.M. Choi, C.R. Ji, Phys. Lett. B **460**, 461 (1999). [arXiv:hep-ph/9903496](#)
9. W. Jaus, Phys. Rev. D **60**, 054026 (1999)
10. Z.Q. Zhang, Z.J. Sun, Y.C. Zhao, Y.Y. Yang, Z.Y. Zhang, Eur. Phys. J. C **83**, 477 (2023). [arXiv:2301.11107](#) [hep-ph]
11. W. Wang, Y.L. Shen, C.D. Lu, Phys. Rev. D **79**, 054012 (2009). [arXiv:0811.3748](#) [hep-ph]
12. H.W. Ke, T. Liu, X.Q. Li, Phys. Rev. D **89**, 017501 (2014). [arXiv:1307.5925](#) [hep-ph]
13. H.Y. Cheng, C.K. Chua, C.W. Hwang, Phys. Rev. D **69**, 074025 (2004). [arXiv:hep-ph/0310359](#)
14. X.X. Wang, W. Wang, C.D. Lu, Phys. Rev. D **79**, 114018 (2009). [arXiv:0901.1934](#) [hep-ph]
15. R. Aaij et al. (LHCb Collaboration), Phys. Rev. Lett. **120**, 121801 (2018). [arXiv:1711.05623](#) [hep-ex]

16. T.D. Cohen, H. Lamm, R.F. Lebed, JHEP **09**, 168 (2018). [arXiv:1807.02730](#) [hep-ph]
17. A. Issadykov, M.A. Ivanov, Phys. Lett. B **783**, 178 (2018). [arXiv:1804.00472](#) [hep-ph]
18. C.F. Qiao, R.L. Zhu, Phys. Rev. D **87**, 014009 (2013). [arXiv:1208.5916](#) [hep-ph]
19. C.F. Qiao, P. Sun, D. Yang, R.L. Zhu, Phys. Rev. D **89**, 034008 (2014). [arXiv:1209.5859](#) [hep-ph]
20. C.H. Chang, H.F. Fu, G.L. Wang, J.M. Zhang, Sci. China Phys. Mech. Astron. **58**, 071001 (2015). [arXiv:1411.3428](#) [hep-ph]
21. T. Zhou, T.H. Wang, Y. Jiang, L. Huo, G.L. Wang, J. Phys. G **48**, 055006 (2021). [arXiv:2006.05704](#) [hep-ph]
22. D. Ebert, R.N. Faustov, V.O. Galkin, Phys. Rev. D **68**, 094020 (2003). [arXiv:hep-ph/0306306](#)
23. D. Ebert, R.N. Faustov, V.O. Galkin, Phys. Rev. D **82**, 034019 (2010). [arXiv:1007.1369](#) [hep-ph]
24. M.A. Ivanov, J.G. Korner, P. Santorelli, Phys. Rev. D **73**, 054024 (2006). [arXiv:hep-ph/0602050](#)
25. Y.M. Wang, C.D. Lu, Phys. Rev. D **77**, 054003 (2008). [arXiv:0707.4439](#) [hep-ph]
26. T. Huang, F. Zuo, Eur. Phys. J. C **51**, 833 (2007). [arXiv:hep-ph/0702147](#)
27. A.Y. Anisimov, I.M. Narodetsky, C. Semay, B. Silvestre-Brac, Phys. Lett. B **452**, 129 (1999). [arXiv:hep-ph/9812514](#)
28. A.Y. Anisimov, P.Y. Kulikov, I.M. Narodetsky, K.A. Ter-Martirosian, Phys. Atom. Nucl. **62**, 1739 (1999). [arXiv:hep-ph/9809249](#)
29. E. Hernandez, J. Nieves, J.M. Verde-Velasco, Phys. Rev. D **74**, 074008 (2006). [arXiv:hep-ph/0607150](#)
30. P. Colangelo, F. De Fazio, Phys. Rev. D **61**, 034012 (2000). [arXiv:hep-ph/9909423](#)
31. I. Bediaga, J.H. Munoz, [arXiv:1102.2190](#) [hep-ph]
32. Z. Rui, H. Li, G.X. Wang, Y. Xiao, Eur. Phys. J. C **76**, 564 (2016). [arXiv:1602.08918](#) [hep-ph]
33. W.F. Wang, Y.Y. Fan, Z.J. Xiao, Chin. Phys. C **37**, 093102 (2013). [arXiv:1212.5903](#) [hep-ph]
34. J.F. Sun, D.S. Du, Y.L. Yang, Eur. Phys. J. C **60**, 107 (2009). [arXiv:0808.3619](#) [hep-ph]
35. M.A. Ivanov, J.G. Korner, P. Santorelli, Phys. Rev. D **63**, 074010 (2001). [arXiv:hep-ph/0007169](#)
36. V.V. Kiselev, A.E. Kovalsky, A.K. Likhoded, Nucl. Phys. B **585**, 353 (2000). [arXiv:hep-ph/0002127](#)
37. A. Issadykov, M.A. Ivanov, G. Nurbakova, EPJ Web Conf. **158**, 03002 (2017). [arXiv:1907.13210](#) [hep-ph]
38. L. Nayak, P.C. Dash, S. Kar, N. Barik, Eur. Phys. J. C **82**, 750 (2022). [arXiv:2204.04453](#) [hep-ph]
39. Z.Q. Zhang, Z.L. Guan, Y.C. Zhao, Z.Y. Zhang, Z.J. Sun, N. Wang, X.D. Ren, Chin. Phys. C **47**, 013103 (2023). [arXiv:2208.07990](#) [hep-ph]
40. Y. Sakaki, M. Tanaka, A. Tayduganov, R. Watanabe, Phys. Rev. D **88**, 094012 (2013). [arXiv:1309.0301](#) [hep-ph]
41. R.L. Workman et al. (Particle Data Group), Review of particle physics. PTEP **2022**, 083C01 (2022)
42. A. Berns, H. Lamm, JHEP **12**, 114 (2018). [arXiv:1808.07360](#) [hep-ph]
43. W. Wang, R.L. Zhu, Int. J. Mod. Phys. A **34**, 1950195 (2019). [arXiv:1808.10830](#) [hep-ph]
44. H. Lamm, [arXiv:1809.08227](#) [hep-ph]
45. A. Cerri et al., CERN Yellow Rep. Monogr. **7**, 867 (2019). [arXiv:1812.07638](#) [hep-ph]
46. M. Tanaka, R. Watanabe, Phys. Rev. D **87**, 034028 (2013). [arXiv:1212.1878](#) [hep-ph]
47. J.P. Lees et al. (BaBar Collaboration), Phys. Rev. D **88**, 072012 (2013). [arXiv:1303.0571](#) [hep-ex]
48. M.A. Ivanov, J.G. Korner, C.T. Tran, Phys. Rev. D **92**, 114022 (2015). [arXiv:1508.02678](#) [hep-ph]

49. M.A. Ivanov, J.G. Korner, C.T. Tran, Phys. Rev. D **95**, 036021 (2017). [arXiv:1701.02937](#) [hep-ph]
50. M. Tanaka, R. Watanabe, Phys. Rev. D **82**, 034027 (2010). [arXiv:1005.4306](#) [hep-ph]
51. Y.K. Hsiao, C.Q. Geng, Chin. Phys. C **41**, 013101 (2017). [arXiv:1607.02718](#) [hep-ph]
52. V.V. Kiselev, [arXiv:hep-ph/0211021](#)
53. C.H. Chang, Y.Q. Chen, Phys. Rev. D **49**, 3399 (1994)
54. R.N. Faustov, V.O. Galkin, X.W. Kang, Phys. Rev. D **106**, 013004 (2022). [arXiv:2206.10277](#) [hep-ph]
55. L. Nayak, S. Patnaik, P.C. Dash, S. Kar, N. Barik, Phys. Rev. D **104**, 036012 (2021). [arXiv:2106.09463](#) [hep-ph]
56. Z.R. Huang, Y. Li, C.D. Lu, M.A. Paracha, C. Wang, Phys. Rev. D **98**, 095018 (2018). [arXiv:1808.03565](#) [hep-ph]